Inorganic Chemistry

ARTICLE

pubs.acs.org/IC

Observation of Inductive Effects That Cause a Change in the Rate-Determining Step for the Conversion of Rhenium Azides to Imido Complexes

Nicholas E. Travia,[†,‡] Zhenggang Xu,[§] Jason M. Keith,[§,⊥] Elon A. Ison,[†,¶] Phillip E. Fanwick,[†] Michael B. Hall,[*,§] and Mahdi M. Abu-Omar[*,†]

[†]Brown Laboratory, Department of Chemistry, Purdue University, 560 Oval Drive, West Lafayette, Indiana 47907, United States

[§]Department of Chemistry, Texas A&M University, College Station, Texas 77843-3255, United States

Supporting Information

ABSTRACT: The cationic oxorhenium(V) complex $[Re(O)(hoz)_2(CH_3CN)][B(C_6F_5)_4]$ [**1**; Hhoz = 2-(2′-hydroxyphenyl)-2-oxazoline] reacts with aryl azides (N_3Ar) to give cationic *cis*-rhenium(VII) oxoimido complexes of the general formula $[Re(O)(NAr)(hoz)_2][B(C_6F_5)_4]$ [**2a**−**2f**; Ar = 4-methoxyphenyl, 4-methylphenyl, phenyl, 3-methoxyphenyl, 4-chlorophenyl, and 4-(trifluoromethyl)phenyl]. The kinetics of formation of **2** in CH_3CN are first-order in both azide (N_3Ar) and oxorhenium(V) complex **1**, with second-order rate constants ranging from 3.5×10^{-2} to 1.7×10^{-1} M^{-1} s^{-1}. A strong inductive effect is observed for electron-withdrawing substituents, leading to a negative Hammett reaction constant $\rho = -1.3$. However, electron-donating substituents on phenyl azide deviate significantly from this trend. Enthalpic barriers ($\Delta H^{\ddagger}$) determined by the Eyring−Polanyi equation are in the range 14−19 kcal mol^{-1} for all aryl azides studied. However, electron-donating 4-methoxyphenyl azide exhibits a large negative entropy of activation, $\Delta S^{\ddagger} = -21$ cal mol^{-1} K^{-1}, which is in sharp contrast to the near zero $\Delta S^{\ddagger}$ observed for phenyl azide and 4-(trifluoromethyl)phenyl azide. The Hammett linear free-energy relationship and the activation parameters support a change in the mechanism between electron-withdrawing and electron-donating aryl azides. Density functional theory predicts that the aryl azides coordinate via N_α and extrude N_2 directly. For the electron-withdrawing substituents, N_2 extrusion is rate-determining, while for the electron-donating substituents, the rate-determining step becomes the initial attack of the azide. The barriers for these two steps are inverted in their order with respect to the Hammett σ values; thus, the Hammett plot appears with a break in its slope.

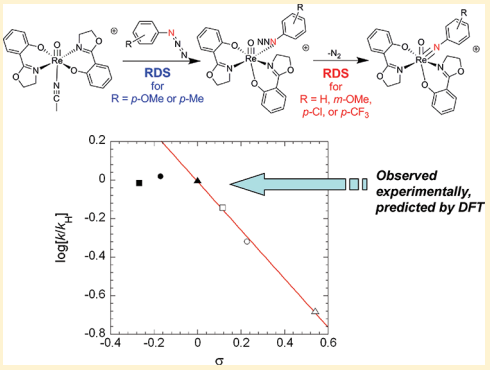

INTRODUCTION

Organic azides, RN_3, have found extensive use in synthetic reactions.[1] Their propensity toward the release of N_2 has enabled their utility as a source of reactive nitrene [RN] species. Therefore, their study has been largely focused on various ways to trap and/or transfer nitrene intermediates for transformations such as amination[2−5] and aziridination.[6−13] More recently, organic azides have gained widespread attention for their metal-catalyzed 1,3-dipolar [3 + 2] cycloaddition to alkynes to give 1,2,3-triazoles,[14−16] a methodology known as "click" chemistry.[17] Many reactions have been realized, thus far, in which [RN] transfer is catalyzed by transition-metal complexes, and in most cases, it is assumed that azide coordinates to the metal center prior to activation. Metal imido [M═NR] intermediates have been invoked in nitrene-transfer reactions. The reactive site of organic azides is the linear NNN moiety, which possesses zwitterionic character. Two resonance forms delocalizing a negative charge between N_α and N_γ can be envisaged (Scheme 1). The bond orders for N_α−N_β and N_β−N_γ are approximately 1.5 and 2.5, respectively (bond lengths of 1.24 and 1.13 Å for HN_3).[18] The internal N_α is more basic[19] and is, therefore, the most likely location for coordination to an electron-poor metal center.

Several examples of isolable organoazide complexes are known.[20−26] They display a variety of resonance forms and binding modes (Scheme 2). Several pathways have been proposed for the formation of metal imido from the reaction of organic azides with transition-metal complexes. In 1967, Kwart and Kahn observed N_2 evolution from benzylsulfonyl azide stirred over copper powder and tentatively proposed a metallocycle intermediate in which copper is coordinated to both N_α and N_γ of the azide.[27] Later, the Lewis acid catalyzed ($AlCl_3$) rearrangement of 1-azidoadamantane was proposed to proceed by aluminum coordination to N_α only.[28] Osborne and Trogler provided mechanistic insight by preparing exclusively $(Cp^*)_2V^{15}NPh$ from a

Received: August 16, 2011
Published: September 09, 2011

Scheme 1. Resonance Forms of Phenyl Azide

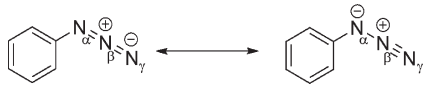

labeled phenyl azide ($Ph^{15}NNN$). They proposed a short-lived intermediate whereby PhN_3 coordinates to vanadium through the labeled N_α to give an η^1-diazoamine complex (Scheme 2b).[29−31] Density functional theory (DFT) computations strongly suggested that copper- and ruthenium-catalyzed 1,3-dipolar cycloaddition to alkynes proceeds through a similar η^1-diazoamine coordination to the metal alkynyl.[32,33] Alternatively, $Cp_2TaMe(N_3Ar)$ and $Cp_2Zr(\mu\text{-}N^tBu)(\mu\text{-}N_3Ph)IrCp^*$ have been suggested to decompose through anti/syn isomerization of the initial diazenimido (Scheme 2d), followed by attack of N_α onto the metal to form a four-membered tetraazametallocyclobutene intermediate.[34] Computational studies demonstrated that both types of intermediates (azametallocycle and diazoamine) are available for the imide formation from $(dtbpe)Ni(\eta^2\text{-}N_3R)$, but a highly negative entropy of activation was more consistent with the four-membered ring azametallocycle pathway.[35]

Cationic rhenium(VII) oxoimido complexes of salen, saldach, and bis(oxazoline) ligand architectures can be prepared by the reaction of aryl azides with mononuclear cationic oxorhenium(V) complexes.[36] The reaction proceeds cleanly at room temperature and features reproducible kinetics with first-order dependence in both rhenium and azide. Drawing from other d^2 examples, we tentatively assigned a mechanism whereby the aryl azide coordinates via the terminal N_γ before proceeding through an azametallocycle analogous to the mechanism described by Bergman for $Cp_2TaMe(N_3Ar)$.[34] Recently, Hall and co-workers offered an alternative mechanism based on DFT computations. The organic azide binds rhenium through the internal N_α to give a η^1-diazoamine intermediate, which extrudes N_2 directly.[37] These computations showed that while a tetraazametallocyclobutene intermediate was accessible for the tantalum complex of Bergman, a prohibitive activation barrier (>50 kcal mol^{-1}) was required for the cationic oxorhenium(V) salen complex. In comparison, the activation energy for direct N_2 extrusion is only 13 kcal mol^{-1}.

In this contribution, we clarify the mechanism of azide reaction with $[Re(O)(hoz)_2(CH_3CN)][B(C_6F_5)_3]$ [**1**; Hhoz = 2-(2′-hydroxyphenyl)-2-oxazolinine; Scheme 3]. Detailed kinetic analysis revealed that the reaction is indeed first-order in rhenium and azide for a variety of electronically substituted aryl azides over a wide range of concentrations. Hammett ρ/σ analysis revealed a drastic change in the electronic effect between electron-donating and -withdrawing aryl substitutions. DFT calculations described herein predict a multistep mechanism involving (1) isomerization of **1**, (2) attack of the azide, (3) N_2 extrusion, and (4) rearrangement of the product, with steps 2 and 3 being rate-determining for electron-donating and -withdrawing substituents, respectively.

EXPERIMENTAL AND COMPUTATIONAL DETAILS

Materials and Methods. Acetonitrile was degassed and purified with a solvent purification system (Anhydrous Engineering Inc.) prior to use. Aniline derivatives and sodium azide were purchased from Aldrich and used as received. Aryl azides were synthesized based on published procedures[38,39] (details in the Supporting Information).

Scheme 2. Coordination Modes of Organic Azides: (a) Terminal Azide Nitrogen (N_γ) Complexation; (b) Coordination through N_α; (c) η^2-Adduct Analogue of Olefin Complexation; (d) Diazenimido and (e) Bridging μ-Imido Ligation

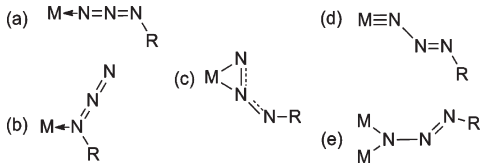

Trityl tetrakis(hexafluorophenyl)borate and trityl hexafluorophosphate were purchased from Strem and used as received. The cationic rhenium oxo complex $[Re(O)(hoz)_2(CH_3CN)][B(C_6F_5)_4]$ (**1**) was synthesized according to published procedures.[40,41] NMR spectra were recorded on Varian Inova 300 instruments. Mass spectrometry was performed by the Purdue University Campus Wide Mass Spectrometry Center. UV−vis spectra were recorded on a Shimadzu UV-2501 spectrophotometer. Stopped-flow kinetics was collected on an Applied Photophysics SX.18MV stopped-flow reaction analyzer. Data fitting was done using *KaleidaGraph 3.0* software.

Computational Details. All of the geometry optimization and frequency determinations were performed with the *Gaussian09* package of programs[42] at the B3LYP level.[43] Transition states were located with use of the synchronous transit-guided, quasi-Newton method.[44] The basis set used for rhenium is the effective-core-potential, extended valence double-ζ LANL2DZ[45] basis, in which the 6p functions were replaced by the reoptimized functions of Couty and Hall,[46] and a set of diffuse f functions (exponent = 0.869) were added.[47] The 6-31G** basis sets were used for all hydrogen, carbon, nitrogen, oxygen, chlorine, and fluorine atoms.[48] Solvation energies were obtained from single-point calculations on gas-phase geometries by applying the SMD solvation model[49] for acetonitrile with default radii and nonelectrostatic terms. The three-dimensional molecular structures were drawn by the *JIMP2* program.[50]

Pseudo-First-Order Kinetics. Equal volumes of solutions of **1** in acetonitrile (5.56 mM) and ArN_3 (Ar = 4-methoxyphenyl, 4-methylphenyl, phenyl, 3-methoxyphenyl, 4-chlorophenyl) were mixed in a stopped-flow analyzer at 298.0 ± 0.2 K to give reaction solutions with half of the loaded concentrations (2.78 mM in rhenium and 0.015−0.30 M in aryl azide). For 4-(trifluoromethyl)phenyl azide, the reaction was slow enough to follow by conventional UV−vis spectrophotometry. **1** in acetonitrile (2.78 mM) and 4-(trifluoromethyl)phenyl azide (0.030−0.30 M) were mixed in a 1.00-cm-path-length quartz UV−vis cell regulated to 298.0 ± 0.2 K. The increase in the absorbance of the rhenium(VII) oxo imido product was monitored at 560 nm. Observed first-order rate constants, k_ψ, were obtained by the nonlinear fitting of A_{560} versus time to the equation $Abs_t = Abs_\infty + (Abs_0 - Abs_\infty)\exp(-k_\psi t)$. Plots of k_ψ versus [aryl azide] were linear, consistent with a first-order dependence on aryl azides (Figure 1). Fits of the data to the rate law $d[\mathbf{2}]/dt = k[\mathbf{1}][ArN_3]$ yielded a second-order rate constant (k) for each aryl azide (Table 1).

Temperature-Dependent Studies. Equal volumes of solutions of **1** in acetonitrile (5.56 mM) and ArN_3 (0.222 M for 4-methoxyphenyl azide and 0.0522 M for phenyl azide) were mixed in the stopped-flow analyzer at temperatures over the range (280.0−313.0) ± 0.2 K to give reaction solutions with half of the loaded concentrations (2.78 mM in **1**, and 0.111 and 0.0261 M in aryl azide). **1** in acetonitrile (2.78 mM) and 4-(trifluoromethyl)phenyl azide (0.049 M) were mixed in a 1-cm-path-length quartz cell regulated to temperatures over the range (285.0−318.0) ± 0.2 K. The increase in the absorbance due to the formation of **2a**, **2c**, or

dx.doi.org/10.1021/ic2017853 |*Inorg. Chem.* 2011, 50, 10505–10514

Scheme 3. Formation of Rhenium(VII) Oxoimido Complexes

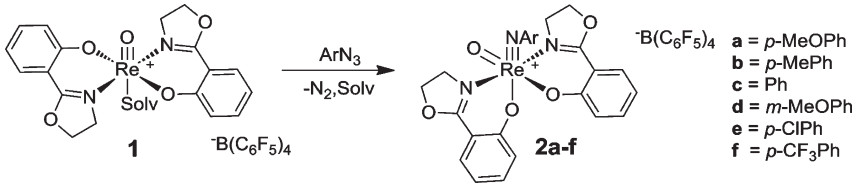

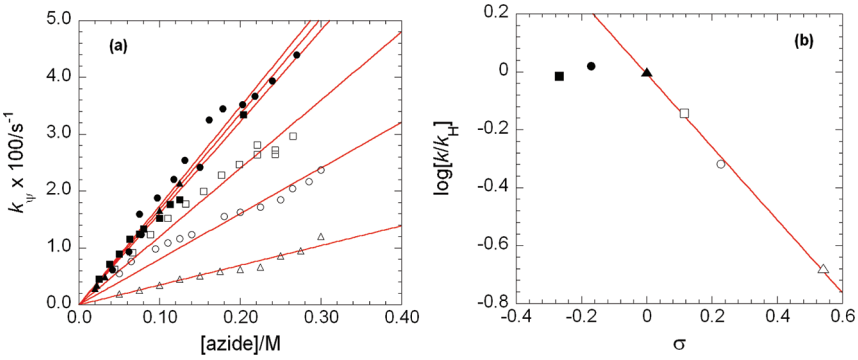

Figure 1. Plots of (a) the pseudo-first-order rate constant, k_ψ, versus [aryl azide] and (b) Hammett relationship for aryl azides with substituents, with the fit showing a linear relationship for electron-withdrawing substituents. Key: ■, *p*-MeO; ●, *p*-Me; ▲, H; □, *m*-MeO; ○, *p*-Cl; Δ, *p*-CF_3. Data collected in CH_3CN at 560 nm and 25.0 ± 0.2 °C.

Table 1. Second-Order Rate Constants and Selected Activation Parameters for the Formation of 2a−2f[a]

Entry	Aryl azide	k/ M^{-1} s^{-1}	$\Delta H^{\ddagger}$/ kcal mol^{-1}	$\Delta S^{\ddagger}$/ cal $mol^{-1}K^{-1}$
1	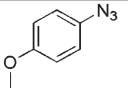	0.161 ± 0.003	14.8 ± 0.8	-21 ± 3
2	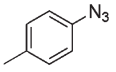	0.174 ± 0.004		
3		0.167 ± 0.003	19 ± 1	-6 ± 4
4	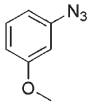	0.120 ± 0.003		
5	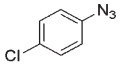	0.080 ± 0.002		
6[b]	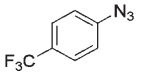	0.035 ± 0.002	18.8 ± 0.6	-9 ± 2

[a] Pseudo-first-order conditions, 2.78 mM **1**, 0.030−0.30 M aryl azide, ArN_3, in CH_3CN at 25.0 ± 0.2 °C. Data were collected at 560 nm using a stopped-flow analyzer. [b] Conventional UV−vis spectrometry at 560 nm.

2f was monitored at 560 nm under pseudo-first-order conditions. The k_ψ values were obtained by the nonlinear fitting of A_{560} versus time to the equation $Abs_t = Abs_\infty + (Abs_0 - Abs_\infty)\exp(-k_\psi t)$. Plots of $\ln(k_\psi/T)$ versus $1/T$ were linear (Figure 2). Fits to the Eyring equation $\ln(k_\psi/T) = -(\Delta H^{\ddagger}/R)(1/T) + (\Delta S^{\ddagger}/R) + \ln(k_B/h)$ gave values for the activation parameters $\Delta H^{\ddagger}$ and $\Delta S^{\ddagger}$.

RESULTS

Kinetics of the Reaction of Cationic Oxorhenium(V) 1 with Aryl Azides, ArN_3. The reaction of **1** with excess ArN_3 in CH_3CN or CH_2Cl_2 gave a change in color from green to intense red, corresponding to a change in the oxidation state from Re^V to

Re^{VII}.[36] After isolation, **2a**−**2f** were recovered in high yields, characterized to be the oxoimido complexes by electrospray ionization mass spectrometry (ESI-MS), and confirmed to be pure by ^{1}H NMR. The pseudo-first-order kinetics of Re^{VII} formation by >10-fold excess azide in CH_3CN was monitored by stopped-flow or conventional UV−vis spectrometry at 560 nm and 25.0 ± 0.2 °C for a series of electron-donating and -withdrawing aryl azides. In all cases, product formation showed first-order dependence on the limiting reagent **1**, and plots of k_ψ versus $[ArN_3]$ were linear with fits passing through the origin (Figure 1a). The slopes from Figure 1a provided second-order rate constants, k, tabulated in Table 1. Saturation kinetics was not observed for any of the azide substrates over a wide concentration range. At very high azide concentrations (>0.50 M), the kinetic profiles deviated from strict first-order kinetics (data not included in the fit), although the values of k_ψ remained consistent with the fitted data in Figure 1a.

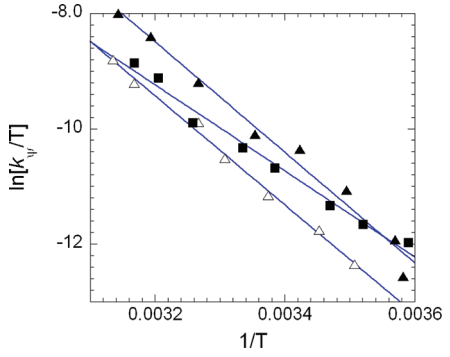

Figure 2. Temperature dependence for the formation of (■) **2a**, (▲) **2c**, and (△) **2f**.

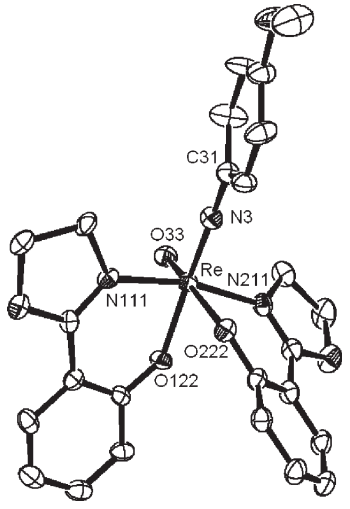

Figure 3. ORTEP molecular structure representation of [**2a**][PF_6]. Thermal ellipsoids are shown at 40% probability. Hydrogen atoms and the anion have been omitted for clarity.

Linear Free-Energy Relationship and Activation Parameters. The Hammett ρ/σ analysis was used to measure the inductive effect of electronic substitutions on the rate of reaction.[51] A plot of $\log(k/k_H)$ versus substituent constant σ for para- and meta-substituted aryl azides showed a linear correlation for electron-withdrawing substituents p-CF_3, p-Cl, and m-MeO passing through the value for PhN_3 with a slope, with reaction constant $\rho = -1.3 \pm 0.1$ suggesting a strong inductive effect as the reaction is accelerated by electron donation on the arene. Surprisingly, for aryl azides with electron-donating substituents, p-Me and p-MeO, the values of k remained nearly unchanged from that of PhN_3 (Figure 1b).

The kinetics remained clean and first-order for all temperatures up to ca. 50 °C before azide thermal decomposition began to compete with the reaction under investigation. Thermodynamic activation constants for the formation of **2a** (p-$OMePhN_3$), **2c** (PhN_3), and **2f** (p-CF_3PhN_3) were determined by the Eyring method over a 35 °C range to give nearly identical values for **2c** ($\Delta H^\ddagger = 19 \pm 1$ kcal mol^{-1}; $\Delta S^\ddagger = -6 \pm 4$ cal mol^{-1} K^{-1}) and **2f** ($\Delta H^\ddagger = 18.8 \pm 0.6$ kcal mol^{-1}; $\Delta S^\ddagger = -9 \pm 2$ cal mol^{-1} K^{-1}); however, **2a** exhibited less enthalpic and more pronounced entropic barriers ($\Delta H^\ddagger = 14.8 \pm 0.8$ kcal mol^{-1}; $\Delta S^\ddagger = -21 \pm 3$ cal mol^{-1} K^{-1}; Figure 2 and Table 1).

Characterization of Complexes 2a−2f. After isolation, **2a**−**2f** were recovered in high yields and characterized by ESI-MS to be the oxoimido complexes. ^{1}H NMR spectroscopy supported a *cis*-oxoimido orientation for all complexes with broken symmetry in the hoz ligand aromatic region. Spectra of these compounds showed distinguishing features different from structurally similar *cis*-$ReO_2(hoz)_2^+$ and *cis*-$Re(O)(hoz)_2Cl$ complexes[36,52] highlighted by two aromatic doublets (one proton each) shifted significantly upfield (δ 6.31−6.18) and a qualitatively different splitting pattern for the oxazoline methylene protons. Aromatic and substituent protons on the imido moiety were shifted downfield relative to the free azide ArN_3.

Multiple attempts to crystallize [**2a**−**2f**][$B(C_6F_5)_4$] failed to yield single crystals suitable for X-ray diffraction. Hence, [**1**]-[PF_6] was prepared from the metathesis reaction of Re(O)-$(hoz)_2Cl$ and trityl hexafluorophosphate. The reaction of [**1**]-[PF_6] with a slight excess of p-$MeOPhN_3$ in acetonitrile yielded a deep-red solution. Suitable crystals of the product were obtained

Table 2. Comparison between the Crystal and Computed Structures for Selected Bond Lengths (Å) and Angles (deg) for 2a

	exp	calc		exp	calc		exp	calc
Re−O33	1.716	1.699	C31−N3−Re	168.2	160.9	N3−Re−N111	90.2	91.2
Re−N3	1.763	1.772	O33−Re−N3	101.7	101.8	O122−Re−N111	84.9	84.2
Re−O122	2.016	2.015	O33−Re−O122	89.5	91.0	O222−Re−N111	91.1	92.3
Re−N111	2.081	2.075	N3−Re−O122	168.4	167.0	O33−Re−N211	86.7	86.3
Re−N211	2.103	2.124	O33−Re−O222	164.9	164.2	N3−Re−N211	99.2	97.1
			N3−Re−O222	88.8	88.3	O122−Re−N211	84.3	86.0
			O122−Re−O222	80.8	79.8	O222−Re−N211	80.9	80.3
			O33−Re−N111	99.7	99.6	N111−Re−N211	167.4	168.6
			C31−N3−Re-O33	152.4	173.1			

dx.doi.org/10.1021/ic2017853 |*Inorg. Chem.* 2011, 50, 10505–10514

by the vapor diffusion of diethyl ether into a concentrated acetonitrile solution at room temperature. Complex **2a** adopts a distorted octahedral geometry, with the angles around rhenium ranging from 80° to 168° (Figure 3 and Table 2). The rhenium imido bond is linear Re−N3−C31 [168.2(6)°], Re−N30 = 1.751(4) Å, and Re−O = 1.714(3) Å, which are within the normal range for Re(heteroatom) multiple bonds.[53−57] The Re−O bond length is identical with that of the analogous $[Re(O)(NMes)(saldach)][B(C_6F_5)_4]$ complex[36] and longer than that of the cationic oxorhenium(V) complexes [*cis*-Re(O)-(saldach)(H_2O)]$[B(C_6F_5)_4]$ [1.664(3) Å][41] and aqua [**1**][OTf] [1.679(7) Å].[52] Re−O bonds trans to multiply bonded ligands are lengthened, Re−O122 = 2.016(5) Å trans to imido and Re−O222 = 2.024(5) Å trans to oxo, per the trans influence expected for multiply bonded ligands.

DFT Results. The rhenium(V) reactant **1** can bind an azide in two possible modes to form intermediates **3_*α*** and **3_*γ*** (Scheme 4). **3_*γ*** is lower in energy than **3_*α***, in part because of steric crowding in **3_*α***. As described in a previous work,[37] the four-membered ring intermediate proposed in Bergman's mechanism,[20,34] where the N_α in **3_*γ*** bends over and also binds to the metal before losing N_2, is highly unfavorable in energy ($\Delta G^{\ddagger}_{sol}$ > 50 kcal mol^{-1}) because the seven-coordinate species is both sterically crowded and a 20 e$^-$ species if it maintains the Re≡O bond. Thus, Bergman's mechanism is very unlikely for this system but is viable with coordinatively and electronically unsaturated early metals. Here, the *α*-bonding intermediate, which extrudes N_2 directly via the previously proposed mechanism,[37] dominates the reaction.

As a first step, the structure of the experimentally determined product, $[Re(O)(p\text{-MeOPhN})(hoz)_2]$ (**2a**), was optimized as described above, and some selected bond lengths and angles are compared to those of the crystal structure in Table 2. The agreement is fairly good, with the largest error in the bond lengths being 0.02 Å, while the largest angular errors occur for C31−N3−Re and the C31−N3−Re−O33 dihedral angle. Optimizing the structure of this product with other functionals yielded similar values for these two angles (see Table S1 in the Supporting Information). One might attribute these angular differences to packing effects within the crystal as our structures are optimized in the gas phase.

Although the structures of the reactant and other products have not been determined, all possible isomers for reactant **1** and the simplest product **2c** were optimized. The reactant **1** has two isomers, for which the two equatorial oxazoline nitrogen atoms occupy trans and cis positions, **1_*trans*** and **1_*cis*** (Figure 4). Because of the repulsion between the hydrogen atoms on the two

Scheme 4. *α* and *γ* Intermediates of Rhenium

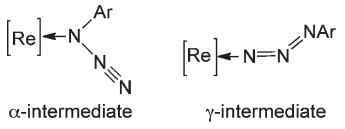

Scheme 5. Different Isomers of Product 2a−2f

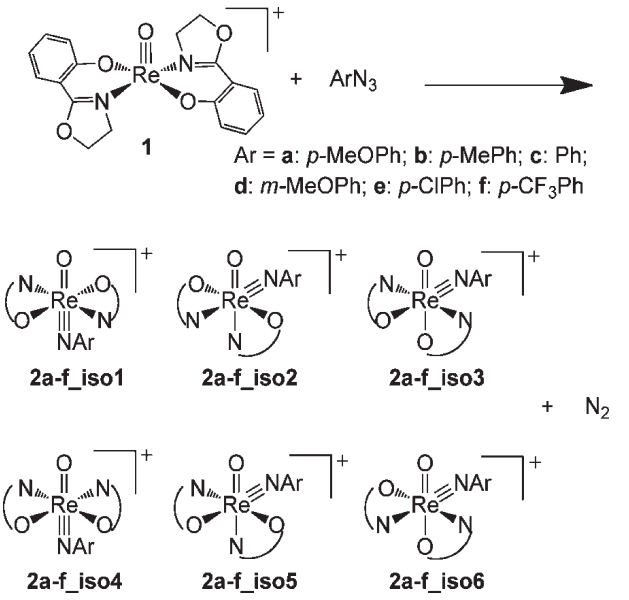

Table 3. Reaction Energies for Different Isomers of 2c Relative to 1_*trans* + PhN_3 (kcal mol^{-1})

	2c_iso1	2c_iso2	2c_iso3	2c_iso4	2c_iso5	2c_iso6
ΔE_{elec}[a1]	−18.86	−44.73	−47.42	−19.22	−39.76	−46.76
ΔH[a2]	−19.65	−45.49	−48.06	−20.07	−40.54	−47.43
ΔG_{gas}[a3]	−17.62	−45.65	−46.42	−18.82	−39.52	−46.61
ΔG_{sol}[a4]	−13.20	−39.97	−40.83	−14.00	−37.85	−41.20
$\Delta G^{\ddagger}_{sol}$[b]	42.15	29.59	32.63	46.13	33.27	24.30

[a] Electronic energies (1), enthalpies (2), gas-phase free energies (3), and solvated free energies (4) for different isomers of the product. All energies are relative to the initial reactants **1** and PhN_3. [b] The free-energy barriers for elimination of N_2 in different pathways to form the various product isomers **2c_iso1−6** relative to the initial reactants **1** and PhN_3.

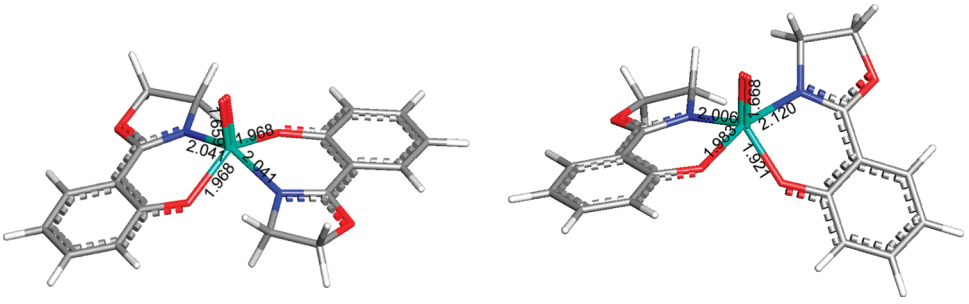

Figure 4. Structures and some selected bonds lengths of **1_*trans*** (left) and **1_*cis*** (right). The ligands lying in the equatorial plane are relatively flat in **1_*trans*** and fairly twisted in **1_*cis***.

dx.doi.org/10.1021/ic2017853 |*Inorg. Chem.* 2011, 50, 10505–10514

Table 4. Comparisons of Energy between iso3 and iso6 for 2a−2f (kcal mol^{-1})

	iso6−iso3					
	2a	**2b**	**2c**	**2d**	**2e**	**2f**
ΔE_{elec}	0.48	0.61	0.66	0.70	0.68	0.77
ΔH	0.46	0.54	0.63	0.64	0.61	0.70
ΔG_{gas}	−0.13	−0.27	−0.19	−0.09	−0.26	0.39
ΔG_{sol}	−0.11	−0.37	−0.37	−0.21	−0.40	0.15

nitrogen atoms in **1_*cis***, the ligands in the equatorial plane adopt a twisted conformation that contributes to making **1_*cis*** higher in free energy than **1_*trans*** by 8.5 kcal mol^{-1}. The imido product **2** from the reaction between **1** and an azide could exist in six possible isomers (**2_iso1−6**; see Scheme 5). The reaction energies for the formation of **2c_iso1−6** (see Table 3) can be rationalized to some extent by the trans influence. The O≡Re triple bond uses the d_{z^2}, d_{xz}, and d_{yz} orbitals of rhenium, so it is particularly difficult for the imido nitrogen to bond trans to oxo, so **2c_iso1** and **2c_iso4** are significantly higher in energy than the other isomers. Because the alkoxide O−Re bond has more ionic character than imine coordination to a Re bond, among the other four isomers, the ones with O trans to oxo (**2c_iso3** and **2c_iso6**) are more stable than those with N trans to oxo (**2c_iso2** and **2c_iso5**). However, the energies of these four isomers, and particularly the two most stable ones, are quite close. Because the differences are so small, the preferred arrangement of ligands in these isomers may be influenced by aspects other than the trans influence.

The similarity in the relative energies for the two most stable isomers, **2_iso3** and **2_iso6**, seen above for **2c** is true for all of the products **2a−2f** (see Table 4). The **2_iso3** isomers are lower in electronic energy than the **2_iso6** isomers for all six substituents. The crystal structure obtained for **2a** corresponds to the computed structure **2a_iso3**, an observation that suggests that the final products prefer the **iso3** structure. On the other hand, the computational results predict that **2_iso6** isomers have lower solvated free energies than **2_iso3** isomers for all species except **2f**. Because of the increased number of approximations involved in the calculation of H and G_{sol}, such as the harmonic approximation for vibrational frequencies and implicit solvation model, the electronic energy differences may more accurately reflect the preferred solid-state structure (different functionals also produce similar results; see Table S3 in the Supporting Information). Thus, we will assume that **2_iso3** isomers represent the final products in accordance with experiment. The energy barriers for rearrangement between isomers **2_iso6** and **2_iso3** are computed to be ∼24 kcal mol^{-1} (see Figure 5). Thus, their rearrangement could occur at room temperature; furthermore, the alternative final product does not influence the rate of the reaction for the mechanism described below because this rearrangement would occur after formation of the very stable products.

In the reaction examined here, the reactant **1** first binds an azide molecule to form intermediate **3_*α***, which then extrudes N_2 directly to yield the desired product **2**. Because several different isomers of the intermediates and products need to be considered, we will refer to the paths for each of the various isomeric products by using the isomer label of the product. For example, path 6 is the reaction path from **1** + azide to the product **2_iso6**. We begin by noting that, in paths 1−3, **1_*trans*** can

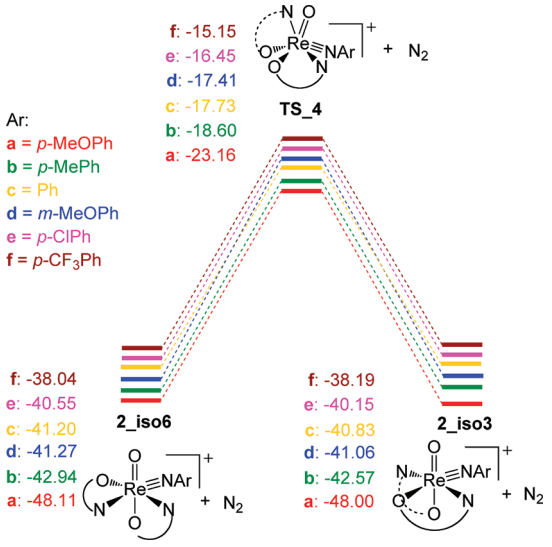

Figure 5. Rearrangement between **2_iso6** and **2_iso3**.

directly bind an azide to form **3_*α*_iso1−3**, while in paths 4−6, **1_*trans*** isomerizes to **1_*cis*** before coordinating an azide molecule. The results in Table 3 show that the lowest free-energy barrier, $\Delta G^{\ddagger}_{sol}$, between **1** + azide and **2c** exists in path 6, indicating that path 6 is the most probable. Although the next highest barrier (path 2) is only ∼5 kcal mol^{-1} higher, DFT energy differences for the barriers of these two very similar steps, extruding N_2, should be accurate enough to eliminate all paths but path 6 from further consideration because the experimental $\Delta G^{\ddagger}$ values span a range of only 2 kcal mol^{-1}.

A detailed free-energy profile for the reaction between **1** and all six substituted azides through path 6 is shown in Figure 6. The profile shows three barriers with similar free energies between the reactants **1_*trans*** + azide and the initial product **2_iso6a-f**. These transition states correspond to **TS-1**, the **1_*trans*** to **1_*cis*** isomerization, which is necessary to access the lowest energy path for the remainder of the reaction (path 6), **TS-2**, the attack of the azide on **1_*cis***, which distorts to accommodate the incoming azide, and **TS-3**, the extrusion of N_2 to form the product. Because the two intermediates, **1_*cis*** + azide and **3_*α*_iso6**, are similarly less stable than the reactant **1_*trans*** + azide and because the product is much more stable, the rate-determining step should correspond to the highest point on the free-energy profile. Close examination of Figure 6 shows that **TS-1** is always lower in energy than the rate-determining step, which varies between **TS-2** and **TS-3** depending on the azide. Thus, isomerization of the reactant never serves as a rate-determining step in the reactions, a conclusion in agreement with the experimental result that all of the reactions are first-order in both azide and the rhenium complex. The observed second-order rate constant corresponds to the transition-state theory expression for the highest remaining barrier, **TS-2** or **TS-3**.

The first of the two key free-energy barriers, **TS-2**, corresponds to attack of the azide in the forward direction or loss of azide from the six-coordinate intermediate, **3_*α*_iso6**, in the backdirection. On the electronic energy surface, **3_*α*_iso6** is more stable than **1_*cis*** + azide, while the entropy loss in forming **3_*α*_iso6** from **1_*cis*** + azide results in a higher free energy for **3_*α*_iso6**, as shown in Figure 6. A scan of the electronic energy for removal of the bound azide from **3_*α*_iso6** results in a

dx.doi.org/10.1021/ic2017853 |*Inorg. Chem.* 2011, 50, 10505–10514

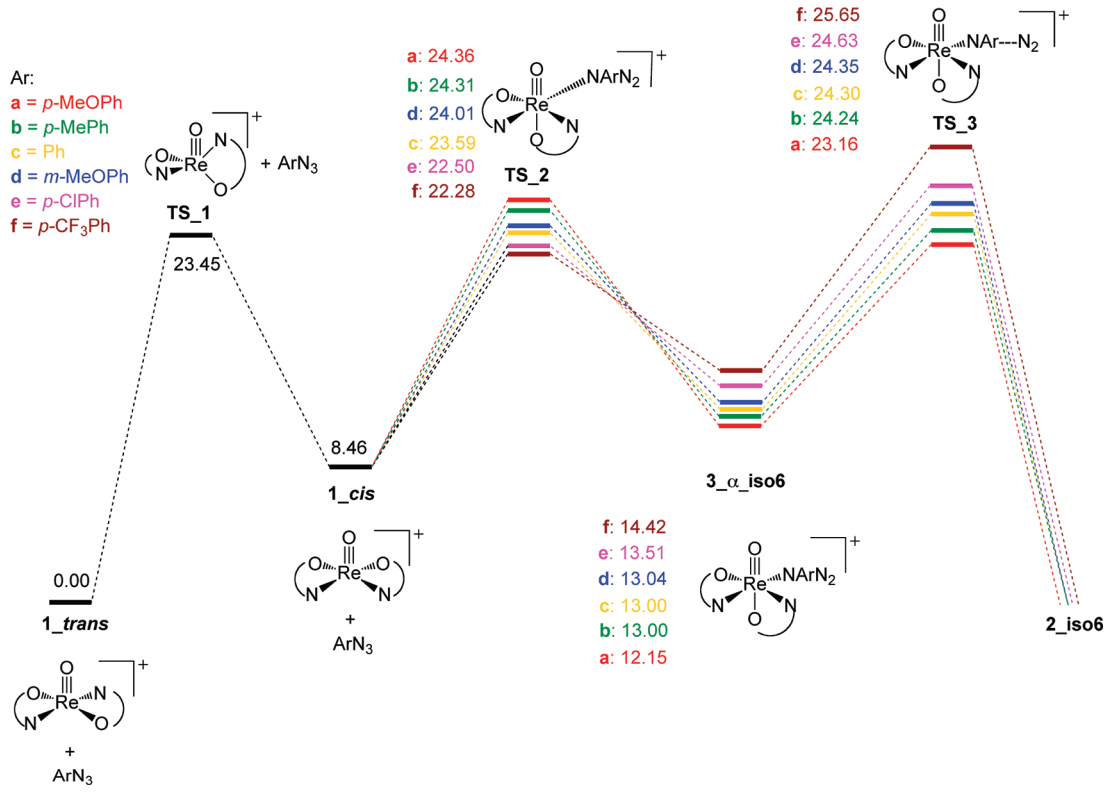

Figure 6. Solvated ΔG (kcal mol^{-1}) diagram for the reaction of the rhenium oxo complex with ArN_3 (solvent: CH_3CN).

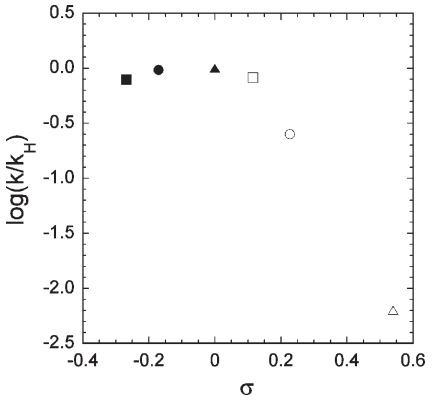

Figure 7. Computed Hammett plot showing fairly good agreement with the experimental plot. Key: ■, *p*-OMe; ●, *p*-Me; ▲, H; □, *m*-OMe; ○, *p*-Cl; △, *p*-CF_3. The $\log(k/k_H)$ is computed from $\Delta G^{\ddagger}_{sol}$ in Figure 6 using the standard TS theory.

smooth increase in the energy as the system returns to **1_*cis*** + azide (see Figure S3 in the Supporting Information). Thus, the free-energy barrier for the loss of azide from **3_*α*_iso6** is dominated by the enthalpy difference between **3_*α*_iso6** and **1_*cis*** + azide, so **TS-2** is located on the free-energy profile at this energy.[58] Because of this relationship, the order of **TS-2**'s free-energy barriers corresponds inversely to the order of the stability for the intermediate, **3_*α*_iso6**, so the most stable intermediate, **3_*α*_iso6**, has the highest barrier for the loss of azide. The second key free-energy barrier, **TS-3**, corresponds to the extrusion of N_2 from the intermediate **3_*α*_iso6**. Here, the most stable intermediate, **3_*α*_iso6**, is further along the reaction coordinate toward products and, hence, has the lowest barrier to N_2 loss. Thus, the order of the free-energy barriers for **TS-3** corresponds directly to the order of the stability for the intermediate, **3_*α*_iso6**.

The source of the "break" in the slope of the Hammett plot lies in the inverted order of the similar magnitude barriers for **TS-2** and **TS-3** for the different azides, **2a**–**2f**. So, for **TS-2**, the order from highest to lowest barrier is **2a** to **2f**, while for **TS-3**, the order is **2f** to **2a**. This inverted order is easily explained by the stability of the intermediate **3_*α*_iso6**. Because this species is the bound azide adduct, the least strongly bound azide, **2f**, will be both the easiest to remove and the most difficult to react to product. Thus, for reactions between **1_*cis*** and (**2f**) *p*-CF_3PhN_3, (**2e**) *p*-$ClPhN_3$, (**2d**) *m*-$MeOPhN_3$, and (**2c**) PhN_3, the rate-determining step is the extrusion of N_2 (**TS-3**). However, for the other two azides, (**2a**) *p*-$MeOPhN_3$ and (**2b**) *p*-$MePhN_3$, the rate-determining step switches to the adduct formation (**TS-2**). It is this change of the rate-determining step that results in these two points having a different slope in the computed Hammett plot (Figure 7). One can also observe corresponding trends in the bond distances that reinforce these conclusions. For example, the least stable **3_*α*_iso6** intermediate, (**f**) *p*-CF_3ArN_3, has a ReN bond length of 2.246 Å, while the most stable one, (**a**) *p*-$MeOArN_3$, has a ReN distance of 2.208 Å. Thus, the most stable **3_*α*_iso6** intermediate (**a**) has the shortest (and strongest) ReN bond, which means it will have the most difficult azide to remove (**TS-2**) and it is also the furthest along the forward reaction coordinate and will have the lowest barrier for imido formation (**TS-3**).

Although the energy differences between the various azides for both **TS-2** and **TS-3** are small and less than the absolute accuracy

dx.doi.org/10.1021/ic2017853 |*Inorg. Chem.* 2011, 50, 10505–10514

Scheme 6. Proposed Kinetic Mechanism for the Reaction of ArN_3 with 1

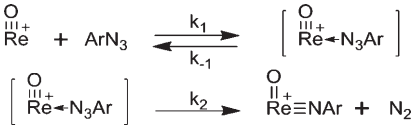

of DFT calculations, DFT typically reproduces such trends much more accurately, as is observed here. Alternative choices for the functional reproduce the trends for the order of the azides **2a**−**2f** for each of the TSs and reproduce the inverse of the order of the free energies within the two transition states discussed above. Furthermore, the range of the experimental rates for the formation of **2a-f_iso6** is consistent with the computed barriers whose range is within 2 kcal mol^{-1}. Because the inductive effect of the substitution should affect the barriers of all paths similarly, the lowest overall barriers for reactions between different substituted azide species and **1** should always be found in path 6, which is more than 5 kcal mol^{-1} lower than the next lowest path. The computed absolute overall barriers are around 25 kcal mol^{-1}, slightly higher than 21 kcal mol^{-1} obtained experimentally, but this systematic error of DFT does not mar the relative trends of concern here. However, one must be cautious about the relative energy of **TS-2** with respect to that of **TS-3** because these two TSs are different in their electronic structure so an alternative functional may shift all of the **TS-2** free energies with respect to those of **TS-3**. Apparently, the B3LYP functional with the basis set and solvation corrections used here places the two transition states at the correct relative energy such that the "break" in the predicted Hammett plot (Figure 7) occurs in the same region as the experimental one (Figure 1). Although other functionals may not produce such accurate results, they would produce the same trends and would result in the same explanation of the experimental results. Thus, it is the judicious combination of experiment and theory that leads to the insight about this mechanism.

DISCUSSION

Analysis of the Kinetic Mechanism. The rate expression for the reaction of aryl azides with **1** implicates a transition state composed of one molecule each of aryl azide and the oxorhenium(V) complex $[\mathbf{1}][B(C_6F_5)_4]$. We have previously reported that, upon treatment with 1 equiv of *p*-CF_3PhN_3 at −80 °C, the analogous oxorhenium(V) saldach complex reacted to give an observable intermediate that yielded the corresponding rhenium(VII) oxoimido product upon warming.[36] We presume a mechanism by which a Re−N_3Ar adduct is formed prior to product formation (Scheme 6), although on the basis of kinetics alone, adduct formation is not mandatory. The rate expression for the mechanism in Scheme 6 assuming steady state for [Re−N_3Ar] is given in eq 1. Both steps are rate-determining, and the experimental second-order rate constants in Table 2 are a composite of $k_1k_2/(k_{-1} + k_2)$. Another kinetically indistinguishable mechanism is the formation of the rhenium azide adduct, [Re−N_3Ar], in an a priori equilibrium followed by extrusion of N_2 in the rate-determining step. The rate law for this scenario is given in eq 2. Because kinetic saturation in [N_3Ar] is not observed, it is reasonable to assume that $k_{-1} \gg k_1[N_3Ar]$ and, hence, the rhenium azide intermediate does not accumulate to appreciable concentrations to allow detection. In this instant, the experimentally determined second-order rate constants would correspond to Kk_2. DFT calculations are consistent with the proposed kinetic mechanism, and they provide new insight on the fast initial trans to cis ligand isomerization in **1** and on the preferred mode of coordination, namely, via N_α of the azide.

$$\frac{d[Re^{VII}]}{dt} = \frac{k_1k_2[Re(O)][ArN_3]}{k_2 + k_{-1}} \quad (1)$$

$$\frac{d[Re^{VII}]}{dt} = \frac{Kk_2[Re]_T[ArN_3]}{1 + K[ArN_3]} \cong Kk_2[Re]_T[ArN_3] \quad (2)$$

Analysis of the Inductive Effect. Even though the kinetic behavior is consistent for all of the aryl azides employed in this study, the abrupt change observed in the Hammett correlation is very informative. Deviations in the linear free-energy relationships often indicate changes in the mechanism.[59] A negative reaction constant ρ is observed for electron-withdrawing substituents on the aryl azide, demonstrating a positive charge buildup in the transition state. We presume that azide coordination to the electron-deficient Re center is accelerated by electron-donating azides. Two coordination modes are considered for the oxorhenium(V) system, (1) diazenylimido through N_γ and (2) a η^1-azide adduct through N_α. The first has been observed by Bergman and Cummins in their respective Ta and V d^2 systems.[20,21] The second has been shown by Wu and Hall by DFT to be the relevant intermediate along the reaction pathway for oxorhenium(V) saldach reaction with phenyl azide[37] and herein for this system and aryl azides with different substituents. In the Bergman mechanism, the reaction is presumed to proceed via an anti/syn rotation about the TaN−NNAr bond followed by rapid generation of a tetraazametallocycle intermediate that extrudes N_2. Electron-withdrawing substituents on phenyl azide strongly accelerated the reaction and ρ = +0.66 was observed. A rate-determining step involving anti/syn isomerization was proposed, and it was argued that the disruption of extended conjugation produced a negative charge buildup on the [ArN^-] fragment. This was supported by the observed activation entropy, $\Delta S^{\ddagger}$ = −0.7 cal mol^{-1} K^{-1}. If our system here follows a mechanism similar to Bergman's, a reasonable explanation of the Hammett analysis would be that, for electron-withdrawing aryl azides, coordination is rate-determining and all subsequent steps are fast. This explanation can be refuted because a near-zero entropy of activation for PhN_3 and *p*-CF_3PhN_3 would make little sense if coordination is rate-determining. In contrast, the mechanism calculated herein by DFT would proceed via N_2 extrusion from an η^1-diazoamine intermediate and would be decelerated by electron-withdrawing aryl substituents. Indeed, the computed reaction profiles for electron-withdrawing aryl azides show that the N_2 extrusion step from the N_α azide adduct is rate-determining (Figure 6). Furthermore, the computed activation barriers are consistent with the observed experimental trend for PhN_3, *m*-$MeOPhN_3$, *p*-$ClPhN_3$, and *p*-CF_3PhN_3.

In order for a mechanism comprised of more than one electronically sensitive elementary step to show a near-zero Hammett reaction constant, two or more electronically influenced steps must be offsetting each other. A possible explanation is a change in the rate-determining step rather than a change in the overall pathway. For the substrates with electron-donating substituents *p*-$MeOPhN_3$ and *p*-$MePhN_3$, the rate-determining step becomes N_α azide adduct formation (Figure 6). The large and negative

entropy of activation measured for *p*-MeOPhN$_3$ ($\Delta S^{\ddagger} = -21$ cal mol^{-1} K^{-1}) is consistent with adduct formation being rate-determining. It should be noted that, even though there is a strong inductive effect from aryl substitutions, the change in the rate-determining step is allowed to occur because the overall barriers are close in energy within 4 kcal mol^{-1}. Had their energies deviated more, the break in the Hammett plot might not have been observed. Thus, the unusual switch in rate-determining steps between **TS_2** and **TS_3**, as revealed by computation (Figure 6), is the result of *both* (1) the close relative barriers of the two steps and (2) the inverted order in the reaction barriers from **2a**−**2f** between coordination and N$_2$ extrusion.

CONCLUSION

We have demonstrated that the reaction of aryl azides with oxorhenium(V) follows overall second-order kinetics and proceeds via a metal azide intermediate. A Hammett study of the electronic effects on this reaction unveiled a deviation from linearity. Aryl azides with electron-withdrawing substituents and PhN$_3$ follow a common trend with a reaction constant $\rho = -1.3$. Aryl azides with electron-donating substituents give a $\rho \approx 0$. DFT computations reveal that all of the reactions follow the direct N$_2$ extrusion mechanism and the same pathway leading to final products. However, the rate-determining step for the formation of **2a**−**2f** switches from the formation of the azide adduct to extrusion of N$_2$ from this adduct. A key to observing this phenomenon is that in this particular case the two barriers are sufficiently close in energy that a change in the substituent causes a change in the rate-determining step. What is remarkable about this particular reaction is not that these two barriers have opposite behavior with respect to their order for a series of substituents, which is essential but easily explained, but that they have such similar barriers that changes in substituents somewhat far from the reacting atoms cause a change in the rate-determining step.

ASSOCIATED CONTENT

Supporting Information. Experimental and computational details and crystallographic data in CIF format. This material is available free of charge via the Internet at http://pubs.acs.org.

AUTHOR INFORMATION

Corresponding Author

*E-mail: hall@science.tamu.edu (M.B.H.), mabuomar@purdue.edu (M.M.A.).

Present Addresses

[‡]Los Alamos National Laboratory, Mail Stop J-514, Los Alamos, NM 87545.

[⊥]Theoretical Division, MS B268, Los Alamos National Laboratory, Los Alamos, NM 87545.

[¶]Department of Chemistry and Biochemistry, North Carolina State University, Box 8204, 2620 Yarbrough Drive, Raleigh, NC 27695.

ACKNOWLEDGMENT

Support of this work was provided by the Chemical Sciences Division, Office of Basic Energy Sciences, U.S. Department of Energy (Grant DE-FG02-06ER15794) and by the Chemistry Division of the National Science Foundation (Grant CHE-0910552) and The Welch Foundation (Grant A-0648).

REFERENCES

(1) Brase, S.; Gil, C.; Knepper, K.; Zimmermann, V. *Angew. Chem., Int. Ed.* **2005**, *44*, 5188.
(2) Cenini, S.; Gallo, E.; Caselli, A.; Ragaini, F.; Fantauzzi, S.; Piangiolino, C. *Coord. Chem. Rev.* **2006**, *250*, 1234.
(3) Caselli, A.; Gallo, E.; Fantauzzi, S.; Morlacchi, S.; Ragaini, F.; Cenini, S. *Eur. J. Inorg. Chem.* **2008**, 3009.
(4) Omura, K.; Murakami, M.; Uchida, T.; Irie, R.; Katsuki, T. *Chem. Lett.* **2003**, *32*, 354.
(5) Shen, M. H.; Leslie, B. E.; Driver, T. G. *Angew. Chem., Int. Ed.* **2008**, *47*, 5056.
(6) Fantauzzi, S.; Gallo, E.; Caselli, A.; Piangiolino, C.; Ragaini, F.; Cenini, S. *Eur. J. Org. Chem.* **2007**, 6053.
(7) Fantauzzi, S.; Gallo, E.; Caselli, A.; Ragaini, F.; Macchi, P.; Casati, N.; Cenini, S. *Organometallics* **2005**, *24*, 4710.
(8) Gao, G. Y.; Jones, J. E.; Vyas, R.; Harden, J. D.; Zhang, X. P. *J. Org. Chem.* **2006**, *71*, 6655.
(9) Han, H.; Park, S. B.; Kim, S. K.; Chang, S. B. *J. Org. Chem.* **2008**, *73*, 2862.
(10) Jones, J. E.; Ruppel, J. V.; Gao, G. Y.; Moore, T. M.; Zhang, X. P. *J. Org. Chem.* **2008**, *73*, 7260.
(11) Li, J.; Fu, Y.; Guo, Q. X. *Tetrahedron* **2008**, *64*, 11167.
(12) Omura, K.; Uchida, T.; Irie, R.; Katsuki, T. *Chem. Commun.* **2004**, 2060.
(13) Subbarayan, V.; Ruppel, J. V.; Zhu, S.; Perman, J. A.; Zhang, X. P. *Chem. Commun.* **2009**, 4266.
(14) Zhang, L.; Chen, X. G.; Xue, P.; Sun, H. H. Y.; Williams, I. D.; Sharpless, K. B.; Fokin, V. V.; Jia, G. C. *J. Am. Chem. Soc.* **2005**, *127*, 15998.
(15) Rostovtsev, V. V.; Green, L. G.; Fokin, V. V.; Sharpless, K. B. *Angew. Chem., Int. Ed.* **2002**, *41*, 2596.
(16) Tornoe, C. W.; Christensen, C.; Meldal, M. *J. Org. Chem.* **2002**, *67*, 3057.
(17) Kolb, H. C.; Finn, M. G.; Sharpless, K. B. *Angew. Chem., Int. Ed.* **2001**, *40*, 2004.
(18) Winnewisser, M.; Cook, R. L. *J. Chem. Phys.* **1964**, *41*, 999.
(19) Protonation of N_3^- occurs at N_α.Christe, K. O.; Wilson, W. W.; Dixon, D. A.; Khan, S. I.; Bau, R.; Metzenthin, T.; Lu, R. *J. Am. Chem. Soc.* **1993**, *115*, 1836.
(20) Proulx, G.; Bergman, R. G. *J. Am. Chem. Soc.* **1995**, *117*, 6382.
(21) Fickes, M. G.; Davis, W. M.; Cummins, C. C. *J. Am. Chem. Soc.* **1995**, *117*, 6384.
(22) Guillemot, G.; Solari, E.; Floriani, C.; Rizzoli, C. *Organometallics* **2001**, *20*, 607.
(23) Hanna, T. A.; Baranger, A. M.; Bergman, R. G. *Angew. Chem., Int. Ed.* **1996**, *35*, 653.
(24) Albertin, G.; Antoniutti, S.; Bacchi, A.; Celebrin, A.; Pelizzi, G.; Zanardo, G. *Dalton Trans.* **2007**, 661.
(25) Barz, M.; Herdtweck, E.; Thiel, W. R. *Angew. Chem., Int. Ed.* **1998**, *37*, 2262.
(26) Albertin, G.; Antoniutti, S.; Baldan, D.; Castro, J.; Garcia-Fontan, S. *Inorg. Chem.* **2008**, *47*, 742.
(27) Kwart, H.; Kahn, A. A. *J. Am. Chem. Soc.* **1967**, *89*, 1950.
(28) Margosian, D.; Kovacic, P. *J. Org. Chem.* **1981**, *46*, 877.
(29) Gambarotta, S.; Chiesivilla, A.; Guastini, C. *J. Organomet. Chem.* **1984**, *270*, C49.
(30) Osborne, J. H.; Trogler, W. C. *Inorg. Chem.* **1985**, *24*, 3098.
(31) Osborne, J. H.; Rheingold, A. L.; Trogler, W. C. *J. Am. Chem. Soc.* **1985**, *107*, 7945.
(32) Himo, F.; Lovell, T.; Hilgraf, R.; Rostovtsev, V. V.; Noodleman, L.; Sharpless, K. B.; Fokin, V. V. *J. Am. Chem. Soc.* **2005**, *127*, 210.
(33) Bock, V. D.; Hiemstra, H.; van Maarseveen, J. H. *Eur. J. Org. Chem.* **2006**, 51.

(34) Proulx, G.; Bergman, R. G. *Organometallics* **1996**, *15*, 684.
(35) (a) Cundari, T. R.; Morello, G. R. *J. Org. Chem.* **2009**, *74*, 5711. (b) Waterman, R.; Hillhouse, G. L. *J. Am. Chem. Soc.* **2008**, *130*, 12628.
(36) Ison, E. A.; Cessarich, J. E.; Travia, N. E.; Fanwick, P. E.; Abu-Omar, M. M. *J. Am. Chem. Soc.* **2007**, *129*, 1167.
(37) Wu, H.; Hall, M. B. *J. Am. Chem. Soc.* **2008**, *130*, 16452.
(38) Leyva, E.; Munoz, D.; Platz, M. S. *J. Org. Chem.* **1989**, *54*, 5938.
(39) Murata, S.; Abe, S.; Tomioka, H. *J. Org. Chem.* **1997**, *62*, 3055.
(40) McPherson, L. D.; Drees, M.; Khan, S. I.; Strassner, T.; Abu-Omar, M. M. *Inorg. Chem.* **2004**, *43*, 4036.
(41) Ison, E. A.; Cessarich, J. E.; Du, G. D.; Fanwick, P. E.; Abu-Omar, M. M. *Inorg. Chem.* **2006**, *45*, 2385.
(42) Frisch, M. J.; Trucks, G. W.; Schlegel, H. B.; Scuseria, G. E.; Robb, M. A.; Cheeseman, J. R.; Scalmani, G.; Barone, V.; Mennucci, B.; Petersson, G. A.; Nakatsuji, H.; Caricato, M.; Li, X.; Hratchian, H. P.; Izmaylov, A. F.; Bloino, J.; Zheng, G.; Sonnenberg, J. L.; Hada, M.; Ehara, M.; Toyota, K.; Fukuda, R.; Hasegawa, J.; Ishida, M.; Nakajima, T.; Honda, Y.; Kitao, O.; Nakai, H.; Vreven, T.; Montgomery, J. A., Jr.; Peralta, J. E.; Ogliaro, F.; Bearpark, M.; Heyd, J. J.; Brothers, E.; Kudin, K. N.; Staroverov, V. N.; Kobayashi, R.; Normand, J.; Raghavachari, K.; Rendell, A.; Burant, J. C.; Iyengar, S. S.; Tomasi, J.; Cossi, M.; Rega, N.; Millam, J. M.; Klene, M.; Knox, J. E.; Cross, J. B.; Bakken, V.; Adamo, C.; Jaramillo, J.; Gomperts, R.; Stratmann, R. E.; Yazyev, O.; Austin, A. J.; Cammi, R.; Pomelli, C.; Ochterski, J. W.; Martin, R. L.; Morokuma, K.; Zakrzewski, V. G.; Voth, G. A.; Salvador, P.; Dannenberg, J. J.; Dapprich, S.; Daniels, A. D.; Farkas, O.; Foresman, J. B.; Ortiz, J. V.; Cioslowski, J.; Fox, D. J. *Gaussian09*, revision A.02; Gaussian, Inc.: Wallingford, CT, 2009.
(43) (a) Stephens, P. J.; Devlin, F. J.; Chabalowski, C. F.; Frisch, M. *J. Phys. Chem.* **1994**, *98*, 11623. (b) Becke, A. D. *J. Chem. Phys.* **1993**, *98*, 5648. (c) Lee, C.; Yang, W.; Parr, R. G. *Phys. Rev. B* **1988**, *37*, 785.
(44) Peng, C.; Ayala, P. Y.; Schlegel, H. B.; Frisch, M. J. *J. Comput. Chem.* **1996**, *17*, 49.
(45) Hay, P. J.; Wadt, W. R. *J. Chem. Phys.* **1985**, *82*, 299.
(46) Couty, M.; Hall, M. B. *J. Comput. Chem.* **1996**, *17*, 1359.
(47) Ehlers, A. W.; Böhme, M.; Dapprich, S.; Gobbi, A.; Höllwarth, A.; Jonas, V.; Köhler, K. F.; Stegmann, R.; Veldkamp, A.; Frenking, G. *Chem. Phys. Lett.* **1993**, *208*, 111.
(48) (a) Petersson, G. A.; Al-Laham, M. A. *J. Chem. Phys.* **1991**, *94*, 6081. (b) Petersson, G. A.; Bennett, A.; Tensfeldt, T. G.; Al-Laham, M. A.; Shirley, W. A.; Mantzaris, J. *J. Chem. Phys.* **1988**, *89*, 2193. (c) Foresman, J. B.; Frisch, Æ. *Exploring Chemistry with Electronic Structure Methods*, 2nd ed.; Gaussian, Inc.: Pittsburgh, PA, 1996; p 110. The 6-31G(d′) basis set has the d polarization functions for C, N, O, and F taken from the 6-311G basis set, instead of the original arbitrarily assigned value of 0.8 used in the 6-31G(d) basis set.
(49) Marenich, A. V.; Cramer, C. J.; Truhlar, D. G. *J. Phys. Chem. B* **2009**, *113*, 6378.
(50) (a) Manson, J.; Webster, C. E.; Hall, M. B. *JIMP2, a free program for visualizing and manipulating molecules*, version 0.091; Texas A&M University: College Station, TX, 2006. (b) Hall, M. B.; Fenske, R. F. *Inorg. Chem.* **1972**, *11*, 768.
(51) Hammett, L. P. *J. Am. Chem. Soc.* **1937**, *59*, 96.
(52) Arias, J.; Newlands, C. R.; Abu-Omar, M. M. *Inorg. Chem.* **2001**, *40*, 2185.
(53) Espenson, J. H. *Chem. Commun.* **1999**, 479.
(54) Owens, G. S.; Aries, J.; Abu-Omar, M. M. *Catal. Today* **2000**, *55*, 317.
(55) Romao, C. C.; Kuhn, F. E.; Herrmann, W. A. *Chem. Rev.* **1997**, *97*, 3197.
(56) Nugent, W. A.; Mayer, J. M. *Metal−Ligand Multiple Bonds*; Wiley: New York, 1988.
(57) Wigley, D. E. *Prog. Inorg. Chem.* **1994**, *42*, 239.
(58) Hartwig, J. F.; Cook, K. S.; Hapke, M.; Incarvito, C. D.; Fan, Y.; Webster, C. E.; Hall, M. B. *J. Am. Chem. Soc.* **2005**, *127*, 2538.
(59) Apeloig, Y.; Nakash, M. *J. Am. Chem. Soc.* **1996**, *118*, 9798.